Formation of Light Absorbing Soluble Secondary Organics and Insoluble Polymeric Particles from the Dark Reaction of Catechol and Guaiacol with Fe(III)

Samantha Slikboer,[†,∥] Lindsay Grandy,[†,⊥] Sandra L. Blair,[‡,⊥] Sergey A. Nizkorodov,[‡] Richard W. Smith,[§] and Hind A. Al-Abadleh*,[†]
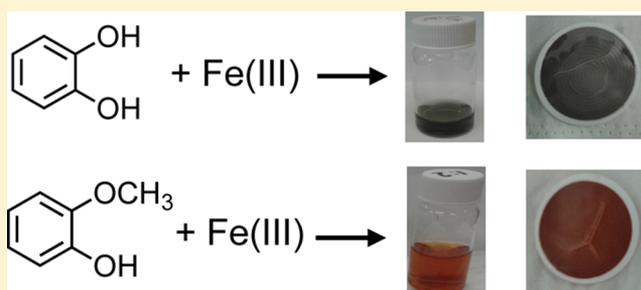
[†]Department of Chemistry and Biochemistry, Wilfrid Laurier University, Waterloo, Ontario N2L 3C5, Canada
[‡]Department of Chemistry, University of California, Irvine, California 92697, United States
[§]University of Waterloo Mass Spectrometry Facility, Department of Chemistry, University of Waterloo, Waterloo, Ontario N2L 3G1, Canada

S *Supporting Information*

ABSTRACT: Transition metals such as iron are reactive components of environmentally relevant surfaces. Here, dark reaction of Fe(III) with catechol and guaiacol was investigated in an aqueous solution at pH 3 under experimental conditions that mimic reactions in the adsorbed phase of water. Using UV–vis spectroscopy, liquid chromatography, mass spectrometry, elemental analysis, dynamic light scattering, and electron microscopy techniques, we characterized the reactants, intermediates, and products as a function of reaction time. The reactions of Fe(III) with catechol and guaiacol produced significant changes in the optical spectra of the solutions due to the formation of light absorbing secondary organics and colloidal organic particles. The primary steps in the reaction mechanism were shown to include oxidation of catechol and guaiacol to hydroxy- and methoxy-quinones. The particles formed within a few minutes of reaction and grew to micron-size aggregates after half an hour reaction. The mass-normalized absorption coefficients of the particles were comparable to those of strongly absorbing brown carbon compounds produced by biomass burning. These results could account for new pathways that lead to atmospheric secondary organic aerosol formation and abiotic polymer formation on environmental surfaces mediated by transition metals.

1. INTRODUCTION

Despite decades of progress in research on atmospheric aerosols, secondary pathways for their formation,[1,2] their role in absorbing and scattering radiation (direct effect on climate), acting as cloud and ice condensation nuclei (indirect effect on the climate),[3] and contributing to heterogeneous chemistry of air pollutants remain active areas of investigation.[4] Given their ubiquitous presence in field-collected aerosols from different origins,[5,6] organic compounds are involved in a number of reactions and processes that transform chemical composition, hygroscopicity, phase, and optical properties of atmospheric aerosols.[7,8] For example, single particle analysis of sea spray particles generated from "ocean-in-a-lab" experiments revealed that under acidic conditions, organic material concentrates at the surface,[9] and that these particles contain transition metals such as iron (Fe).[10] The role of transition metals in the aging and transformation of the organic content on atmospherically relevant surfaces that include aerosols, buildings, and surface water is still unclear and warrants further investigation.[6,11,12]

Aging of organics in aerosols due to heterogeneous chemistry with gas phase oxidants such as O_3, OH, and NO_3 was studied extensively.[2] Dark and photochemical processes driven by

dissolved redox active species such as Fe, OH, H_2O_2, and excited triplet states of certain organics were also investigated in detail with respect to their chemistry in large cloud/fog droplets.[13−15] However, our understanding of oxidation processes relevant to multicomponent atmospheric systems containing sparse amounts of water such as environmental films and wet aerosols is still limited. For example, fluctuations in the water content and acidity of aerosols due to changes in ambient temperature, relative humidity, and reactions with acidic/basic gases affect the solvent−solute ratios and the relative importance of bulk versus surface reactions.[6] Moreover, for some aerosol systems such as mineral dust particles and other atmospherically important surfaces such as buildings, water exists in small pockets of aqueous phase or "adsorbed phase" in the form of islands or films, depending on the underlying substrate and environmental conditions.[11] The high concentrations of solutes in these systems
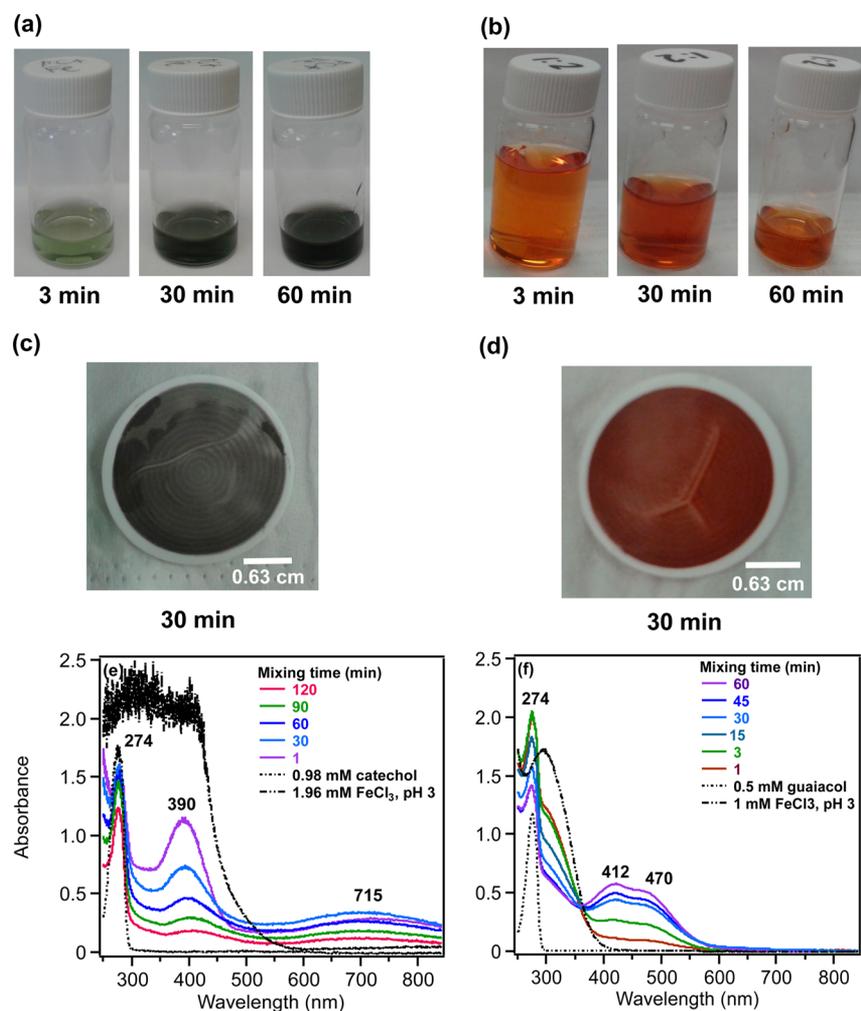
Figure 1. Dark reaction of catechol and guaiacol with FeCl$_3$ at pH 3: (a and b) digital images of 1:2 organic reactant/Fe molar ratio of unfiltered solutions as a function of time; (c and d) particles on filter after 30 min; (e and f) the corresponding UV−vis spectra after filtration.

results in reactions that are uniquely different from the corresponding reactions in more dilute bulk aqueous solutions.[16]

The redox chemistry and strong chelating abilities of Fe in the bulk aqueous phase are well established at the fundamental level[12] and recently were utilized in functionalizing surfaces and nanoparticles for applications in green chemistry[17] and in the development of biomedical and sensing devices.[18−20] In contrast, the role of transition metals such as Fe in driving secondary organic aerosols (SOA) formation from aliphatic and aromatic precursors in heterogeneous/multiphase reactions is not well understood.[1,2,12] This study demonstrates that dark reaction of Fe with catechol and guaiacol under high solute−solvent ratio that mimic reactions in the adsorbed phase of water leads to an efficient redox reaction resulting in complex polymeric products that strongly absorb visible radiation. Catechol and guaiacol (Scheme S1, Supporting Information), are semivolatile phenolic compounds emitted from biomass burning. They are moderately soluble in water with Henry's law constants of 4×10^3 and 900 M atm^{-1}, respectively.[21] These compounds are well-known aromatic SOA precursors[22] and are simple models for the aromatic fraction of humic like substances (HULIS) in aerosols.[22] Catechol, guaiacol, and other catecholates are capable of chelating Fe[19,23] (Scheme S1, Supporting Information), and they easily oxidize to the corresponding quinones (e.g., *o*-quinone in Scheme S1, Supporting Information). Our

observation of the formation of polymeric products, in addition to the expected quinones, could account for new pathways that lead to SOA formation mediated by transition metals, and explain observations from single particle analysis of field-collected "aged" mineral dust aerosol,[11] sea spray from coastal regions impacted by Fe,[10] and abiotic polymer formation on surfaces[24] such as those imaged in sea spray aerosols.[9] Furthermore, this reaction may serve as a source of atmospheric brown carbon−organic aerosol capable of strongly absorbing near-UV and visible radiation translating into direct effect on climate.[25,26]

2. EXPERIMENTAL SECTION

2.1. Chemicals. All chemicals were used as received without further purification: catechol (1,2-benzendiol, >99%, CAS 120-80-9, Sigma-Aldrich), guaiacol (2-methoxyphenol, ≥98%, CAS 90-05-1, Sigma-Aldrich), and iron(III) chloride hexahydrate (FeCl$_3$·6H$_2$O, CAS 10025-77-1, Sigma-Aldrich). Chemicals used as reference compounds and for the hematite dissolution experiments are listed in the Supporting Information. Aqueous phase solutions were prepared by dissolving the chemicals in Milli-Q water (18.5 MΩ cm) or ^{18}O-labeled water (97 atom % ^{18}O, Sigma-Aldrich) with an ionic strength adjusted to 0.01 M by adding potassium chloride (KCl powder, 99.5%, EM Science) to stabilize the pH reading. The pH was adjusted using solutions of

hydrochloric acid (HCl 6 N, Ricca Chemical Company) and sodium hydroxide (NaOH pellets, 99–100%, EMD).

2.2. UV–Visible Spectroscopy and HPLC Experiments. UV–vis spectra were collected using either a fiber optic UV–vis spectrometer (Ocean Optics USB 4000) or a Shimadzu UV-1800 spectrophotometer with a 1 cm quartz cuvette. Chromatograms were collected using a Waters Delta 600 instrument equipped with a Waters 2487 dual wavelength absorbance detector. An in-line degasser was used for sparging at 20 mL/min throughout the experiment to avoid air bubbles. The 4.6 × 250 mm column had Hypersil GOLD C8 stationary phase, with 5 μm particle size, and 175 Å pore size. The mobile phase was flown isocratically using 95% water, with 0.05% TFA and 5% acetonitrile at a flow rate of 1 mL/min. The injection volume of the sample was 30 μL. Further details are provided in the Supporting Information.

2.3. Mass Spectrometric Experiments. Negative ion mode electrospray ionization coupled to liquid chromatography separation (LC-ESI-MS) experiments were performed with a ThermoFisher Scientific Q-Exactive hybrid Orbitrap mass spectrometer. Typical operating conditions are provided in the Supporting Information. Isocratic elution was achieved with 5/95 v/v mixture of acetonitrile/H_2O + 0.1% formic acid. TFA was not used in these experiments because it causes ion suppression in ESI and must be avoided, not just for these studies but also for all subsequent LC/MS analyses. The reaction of chemicals prior to injection was done in a manner similar to that described above for the HPLC experiments.

2.4. Particles Characterization. Particles that formed in the solution as a result of $FeCl_3$ + catechol/guaiacol reaction were collected on nylon membrane filters (0.2 μm pore size, 25 mm dia., EMD) and images of the filters were taken using a digital camera. Mass yield experiments were performed after 2 h reaction using 1:2 molar ratio organic reactant/Fe by weighing the filters before and after filtration followed by overnight drying. For these experiments, the reaction volumes were considerably scaled up (70 mL for catechol/Fe, and 140 mL for guaiacol/Fe) in order to achieve measurable mass yields of particles, keeping the starting concentrations the same in all experiments. The particles were washed with Milli-Q water several times prior to drying. Also, collected filtrates were subjected to filtration four times to ensure minimum loss of particles. The iron content in the particles was analyzed using inductively coupled plasma mass spectrometry (ICP-MS) using method EPA 3050, ALS Global Laboratories. The preparation of samples for scanning electron microscopy-energy dispersive X-ray spectroscopy (SEM-EDS) experiments is described in detail in the Supporting Information. Dynamic light scattering (DLS) experiments were performed on $FeCl_3$ with either catechol or guaiacol reaction solutions in a 1 cm Teflon capped-quartz cuvette with a Malvern Zetasizer Nano (ZEN3600) with settings for each measurement to average 10 runs with a duration of 10 s. For FTIR measurements, the particles were deposited on a ZnSe attenuated total internal reflectance (ATR-FTIR) cell from a water/ethanol slurry followed by drying overnight. Absorbance spectra of these particles were obtained by referencing to the clean and dry ZnSe crystal.

2.5. Acid-Dissolution of Hematite Followed by Reaction with Organics. Hematite nanoparticles were used as a model for iron (oxyhydr)oxides in mineral dust aerosols. A slurry of hematite nanoparticles was prepared in 0.01 M KCl adjusted to pH 1 using HCl, and allowed to mix for 10 days at medium speed in a vortex mixer followed by filtration and determination

of total dissolved iron concentration (see details in the Supporting Information, including Figure S1). After adjusting the pH of the filtrate to 3, catechol or guaiacol was added at half the total iron concentration determined by UV–vis spectroscopy. Samples were allowed to mix in the dark for 60 min prior to filtration and photographing.

3. RESULTS AND DISCUSSION

3.1. Optical Properties and Time Profile of Reactants and Products. Upon reaction of $FeCl_3$ with organics, color development and colloid formation was observed overtime. Figure 1a–d and Figure S2 (Supporting Information) show time-dependent images of solutions and filters resulting from the dark reaction of catechol and guaiacol with $FeCl_3$ at pH 3 in the absence of added oxidants such as H_2O_2. It is important to emphasize here that aqueous solutions are exposed to air, and hence, dissolved O_2 is the oxidant and Fe(III) plays a role as a catalyst. The corresponding UV–vis spectra after filtration (i.e., with particles taken out of the solution) are also shown (Figure 1e,f) and compared to those of the initial spectra of catechol/guaiacol prior to adding $FeCl_3$. While the concentrations are relatively high, they mimic interfacial regions on surfaces where aromatic compounds are enriched at the interface.[27] Both catechol and guaiacol solutions are transparent in the visible range and show a UV band around 274 nm due to $\pi \rightarrow \pi^*$ transitions. The UV–vis absorbance spectrum of $FeCl_3$ solution (pale yellow) shows a band around 295 nm from the ligand-to-metal-charge transfer (LMCT) of the prevailing species in solution, $[Fe(H_2O)_5OH]^{2+}$.[28] Spectra collected at pH = 1–5 exhibit a shift in this peak because the iron speciation is strongly pH-dependent.[29] The pH used in our studies was chosen because a number of studies[29] reported maximum photoreactivity of iron species toward organic degradation at pH 3. These photochemical studies are currently underway in our lab. This pH is also environmentally relevant since aerosols are generally acidic (e.g., pH 3 is possible for fog droplets in highly polluted areas).[13] Studies at pH values lower than 3, which are characteristic of wet aerosols, are currently ongoing in our lab for comparison. In the case of catechol, the initial green color was observed for 1:2, 1:1, and 2:1 organic reactant/Fe molar ratios, attributed to the formation of a bidentate mononuclear catechol–Fe complex (Scheme S1, Supporting Information) with a LMCT band around 700 nm.[30] The intensity of this feature varies with the amount of Fe in the solution mixture, being the least intense for organic reactant/Fe 2:1 solution mixtures. The Fe(III)/Fe(II) cycling can be followed by flow injection analysis and also online by a continuous flow analysis[31,32] where the concentration of Fe(II) and total Fe after the reduction of Fe(III) can be determined on the basis of the color of the reaction as shown in the Supporting Information. This work is currently underway in our laboratories. The intense spectral feature at 390 nm is attributed to n $\rightarrow$ π^* transitions of o-quinone species formed from oxidation of catechol–Fe complexes.[33] We observed this peak at lower concentrations of catechol and iron under acidic conditions and for other catecholates such as gallic acid.[28] The intensity of this feature decreases with less Fe in the solution mixture (Figure S2a,b, Supporting Information, vs Figure 1e). The presence of $-OCH_3$ group in the case of guaiacol inhibits the formation of the iron complex evident by the absence of the characteristic LMCT band in Figure 1f. Instead, spectra in Figure 1f suggest the formation of soluble amber-colored oxidation products (compounds V–VIb; Scheme S1, Supporting Information) due to iron redox chemistry. These spectra are
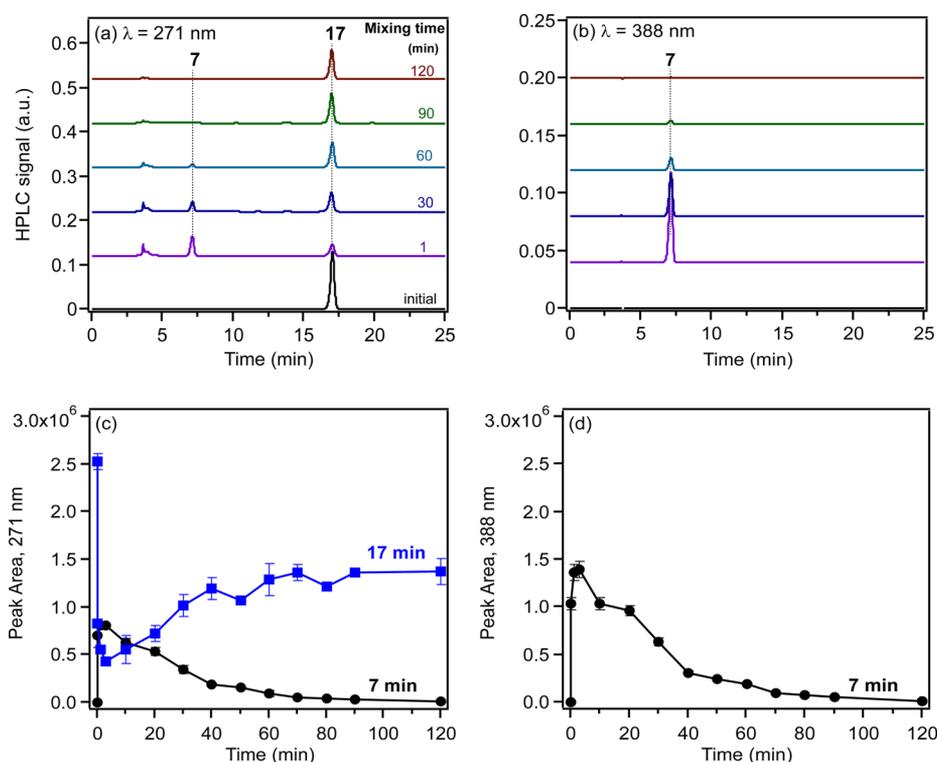
Figure 2. HPLC chromatograms collected at (a) 271 and (b) 388 nm for the initial catechol solutions (0.98 mM) and after reaction with FeCl₃ at pH 3 as a function of reaction time. (c and d) Resulting kinetic curves from the integrated areas of the peaks at 7 and 17 min. The solution mixture contains 1:2 molar ratio of catechol/Fe.

identical to those observed by Hwang et al.[34] who identified products from the biochemical oxidation of guaiacol by manganese peroxidase (MnP) in the presence of H_2O_2 by a suite of analytical techniques. In our study, in situ reduction of Fe(III) to Fe(II) leads to the formation of phenoxy radicals, which proceeds through C−C radical coupling to form compound V. Compounds VIa and VIb (Scheme S1, Supporting Information) give rise to the spectral features at 412 and 470 nm (Figure 1f), which were observed to decrease in intensity upon overnight storage of solutions.[34,35] Schmalzl et al. assigned the 470 nm peak to an unstable 4,4′-diphenoquinone intermediate.[36] Further characterization of guaiacol oxidation products was not carried out herein given the similarities between our data in Figure 1f and published product identification studies.[34,35] Because studies on the oxidation of catechol by Fe(III) are limited under our experimental conditions, the following paragraphs describe in detail the time profile of reactants and products from HPLC studies.

Figure 2 shows HPLC chromatograms collected before and after the addition of FeCl₃ to a catechol solution at pH 3, which were recorded at λ = 271 and 388 nm. These wavelengths were chosen based on UV−vis spectra shown in Figure 1e to separate compounds contributing to the reactant and product peaks. The chromatograms at λ = 271 show two major peaks at 7 and 17 min retention time (RT), whereas only one major peak is present in the chromatograms at λ = 388 nm (RT = 7 min). The 7 and 17 min peaks are assigned to a product and catechol (reactant), respectively, from the comparison with the chromatogram of catechol standard solution. The integrated areas of these peaks are plotted as a function of time in Figure 2c,d for solution mixtures with 1:2 molar ratio of catechol/Fe. Similar experiments were conducted by varying the molar ratios, and the data are presented in Figure S3 (Supporting Information) for 1:1 and 2:1

molar ratios of catechol/Fe. Despite the drop in the performance of the detector at 700 nm, where the catechol−Fe complex absorbs, experiments were conducted to examine the kinetic behavior of the product peak at this wavelength. Figure S4 (Supporting Information) shows results from collecting chromatograms at λ = 700 nm and the resulting kinetic curves for the product peak at 7 min compared with data generated from the chromatograms collected at 271 nm. These kinetic curves track well with each other supporting the assignment of the peak at 7 min to a catechol−Fe complex.

The time profiles of the peak at RT = 7 min clearly show that it is an intermediate species that reaches its maximum concentration at 3 min. Because this product peak has absorptions at 271, 388, and 700 nm, it is consistent with the formation of the catechol−Fe complex and an unstable quinone species that undergoes further oxidation in the presence of dissolved O_2 and excess Fe(III).[30] It is likely that they both exist in equilibrium on the time scale of the collection time. This assignment is also similar to earlier observations of the time profile of peaks in the range 400−500 nm from guaiacol oxidation (see Figure 1). For solution mixtures containing less Fe, as in the 1:1 and 2:1 molar ratios shown in Figure S3 (Supporting Information), a smaller amount of this intermediate is formed, reduced by 50 and 23%, respectively, relative to that in 1:2 catechol/Fe molar ratio solutions. This result suggests that iron plays an important catalytic role in forming this oxidation product of catechol.

In addition, the kinetic curves of the RT = 17 min peak show that it reaches a minimum after 3 min of reaction (~83% decay in catechol, Figure 2c), and then the signal starts to go up due to the contribution of products to the absorbance at λ = 271 nm. These products appear to coelute at the same RT as catechol suggesting similar polarity. Attempts to resolve these peaks using gradient elution were not successful. Lower amounts of Fe in the solution

mixtures with 1:1 and 2:1 molar ratio catechol/Fe resulted in lower decay rates of catechol within the first 3 min (39 and 22%, respectively; Figure S3c, Supporting Information). Scheme S2 (Supporting Information) shows a suggested mechanism for the catechol + Fe(III) reaction based on the data presented herein. This mechanism also explains the formation of polycatechol particles that form over time, which are examined more closely in the last section. To further explore the identity of these products, we describe the results of LC-ESI-MS/MS experiments in the section below.

3.2. Product Identification Using LC-ESI-MS/MS. Figure 3 shows total ion chromatograms (TIC) of a solution mixture
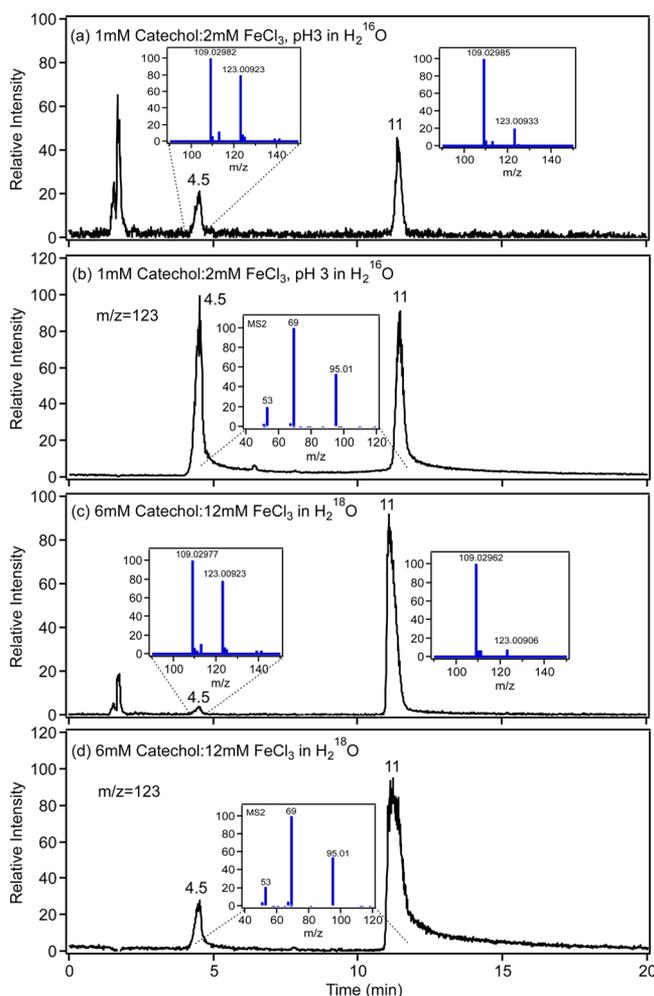

Figure 3. Total ion and m/z 123 LC-ESI-MS/MS negative ion mode chromatograms for the reaction of catechol with $FeCl_3(aq)$ under acidic conditions after 3 min dark reaction in (a and b) normal water ($H_2^{16}O$) and (c and d) ^{18}O-labeled water ($H_2^{18}O$). (a and c, insets) Mass spectra for the major peaks; (b and d, insets) MS/MS spectra for the m/z 123 ion.

containing 1:2 molar ratio of catechol/Fe at pH 3 after reaction for 3 min. The reaction was carried out in normal water ($H_2^{16}O$, Figure 3a,b) and in ^{18}O-labeled water ($H_2^{18}O$, Figure 3c,d) to investigate the source of the oxygen atoms in products containing an added O atom. Similar data were collected for catechol standard solutions, as shown in Figure S5 (Supporting Information). These chromatograms are similar to those collected using HPLC on a separate instrument with a UV−vis detector (Figure 2) with slightly different elution times for the

reactant peak (RT = 11 min) and product peak (RT = 4.5 min). The insets in Figure 3a,c and Figure S5a,c (Supporting Information) show the mass spectra of these major peaks. While ESI-MS/MS detection is not directly quantitative, peak ratios from spectra collected for samples under identical ionization conditions provide insight into the relative amount of a given species. In the absence of $FeCl_3$, the MS spectra of catechol standard solutions (Figure S5, Supporting Information) show the expected $[M-H]^-$ ion peak at m/z 109 ($C_6H_5O_2$) and a peak at m/z 123 ($[M-H]^-$, $C_6H_3O_3$) that coelutes with catechol with a RT of ~11 min (the RT changes slightly in the ^{18}O-labeled water but we are going to refer to this peak as the 11 min peak regardless of the solvent). Note that the 11 min peak elutes later in ^{18}O-labeled water but the eluted compound is the same in both normal and isotopically labeled solvents. The relative ratio of the m/z 109 and m/z 123 is ~100:15 in normal water and 100:6 in ^{18}O-labeled water. As detailed below, the addition of $FeCl_3$ increases the intensity of the m/z 123 peak confirming that it originates from a more oxidized species than catechol. The fragmentation pattern of the m/z 123 from MS/MS spectra is shown in Figures S5b,d (Supporting Information), and it is identical regardless of the isotopic state of water solvent. In general terms, the MS/MS of the m/z 123 fragmentation is identical in intensity, accuracy, ions observed and assigned elemental composition. The absence of mass shifts confirms that the added oxygen atom in the oxidized catechol originates from dissolved O_2 and not water solvent, as suggested earlier.[30]

Catecholates and guaiacol are susceptible to oxidation in the presence of dissolved O_2.[37] Scheme S3 (Supporting Information) shows a likely mechanism that explains the formation of the observed species with m/z 123. The relatively high voltage and ionization conditions under ambient conditions in the ESI chamber may catalyze the formation of radical anions, which, in the presence of $O_2(aq)$, can form hydroxylated quinone species, in the *ortho-* and *para-* positions. Artifacts associated with oxidation and reduction of analytes in ESI sources were not sufficiently studied. Even though the source was polarized for negative ion production, both oxidation and reduction reactions could still occur on the tip of the electrospray capillary. Two reference compounds, 1,2,4-benzenetriol (VII) and pyrogallol (VIII), with the chemical formula $C_6H_6O_3$ were tested to examine the fragmentation pattern of their oxidation products in the ESI chamber. Figure S6 (Supporting Information) shows the chromatograms and MS/MS spectra at pH 3 for these compounds. In Figure S6a (Supporting Information), 1,2,4-benzenetriol shows two peaks with the same fragmentation pattern because it is known to be auto-oxidizible[38] with interconversion between reduced and oxidized occurring over the separation time scale. The likely oxidation steps of 1,2,4-benzenetriol are presented in Scheme S3b (Supporting Information). To explain the two chromatographic peaks with the same MS ion, we collected HPLC/UV−vis chromatograms for 1 mM standard solution of 1,2,4-benzentriol at pH 3. Figure S7 (Supporting Information) shows these results where one chromatographic peak is observed, which is the oxidized form of this molecule. Greenlee et al.[38] developed a method for separation and quantification of phenolic compounds by adding antioxidants and running experiments under oxygen-free conditions using N_2 gas purging. The MS/MS spectrum shown in the inset of Figure S6a (Supporting Information) is identical to that in the insets of Figure 3b,d and Figure S5b,d, Supporting Information. On the other hand, pyrogallol shows one peak in the TIC and in the selected ion chromatogram corresponding to

m/z 123 (Figure S6b, Supporting Information). The fragmentation pattern of this peak (inset) is different than that shown in Figures 3b,d and S5b,d, Supporting Information. Hence, the main conclusion is that autoxidation of catechol takes place to some extent in the ESI source, and the main product is 1,2,4-benzentriol. To the best of the authors' knowledge, the oxidation of catecholates under electrospray ionization conditions was not previously reported.

As detailed above, the addition of FeCl$_3$ to catechol solutions results in complex formation and quinone production. The TICs in Figures 3a,c show a product peak that elutes at RT ~ 4.5 min, with mass spectra containing *m/z* 109 and 123 with 4× and 13× increase in intensity for the latter peak relative to RT ~ 11 min, respectively. Table S1 (Supporting Information) shows that this enhancement in intensity is consistently observed for variable amounts of Fe in solution. These results can be explained in light of the UV−vis and HPLC data presented in the previous section: catechol−Fe complex is more polar (and therefore elutes earlier) than catechol. The complex is not observed mass spectrometrically as it is not stable in the mass spectrometric time frame. As a result, we only see the anionic portion of this complex, that is, the *m/z* 109, which upon formation, is readily oxidized to 1,2,4-benzentriol with *m/z* 123 (identical fragmentation pattern with product peak at RT ~ 4.5 min). Moreover, HPLC/MS experiments were conducted in the positive ion mode under the same elution conditions as negative mode. The resulting spectra yielded no meaningful data because these species do not yield $[M + H]^+$, $[M + Na]^+$, and other positive ions under these solution conditions. Also, the presence of excess Fe(III) in these solutions leads to cluster formation and ion suppression.

Previous studies[34−36] on guaiacol reaction with transition metals including iron characterized some of the soluble products of the oxidation process. Using a combination of HPLC, ^{1}H NMR, fast atom bombardment, and chemical ionization mass spectrometry, Schmalzl et al.[36] studied the reaction of guaiacol with FeCl$_3$ and reported elemental composition, retention times, characteristic chemical shifts, and masses of guaiacol oligomers ranging from dimers to pentamers at 246 (compound V), 368, 490, and 612 mass units. These oligomers formed a precipitate soluble in organic solvents and were found to be mainly organic in composition. Similar oligomers up to trimers were observed in the mass spectra of reaction products from enzymatic oxidation of guaiacol.[34,35] The established mechanism that explains these results is mainly carbon−carbon coupling of guaiacoxy radicals, with little evidence for carbon−oxygen coupling.[34,36] As detailed in the last section, formation of these polymeric species has implications on the overall optical properties and chemical reactivity of the surfaces these products coat.

3.3. Formation of Polymeric Catechol and Guaiacol Particles.

Figure 1c,d shows digital photographs of particles collected on a filter from the dark reaction of catechol and guaiacol with FeCl$_3$ at pH 3. Figure 4 shows SEM images of these particles, which clearly display their amorphous nature as micron-sized conglomerates of nanometer-sized primary particles. EDS experiments showed that polycatechol and polyguaiacol particles are organic and had less than 0.5 atomic % Fe, which was most likely due to contamination from its salt remaining after washing the particles with water. The iron content in these particles analyzed by ICP-MS was also below the detection limit, similar to the results of the control filter with no particles. Moreover, changes in particle size with reaction time was monitored using DLS experiments, which showed that particles appeared within 3 min of the reaction of FeCl$_3$ with
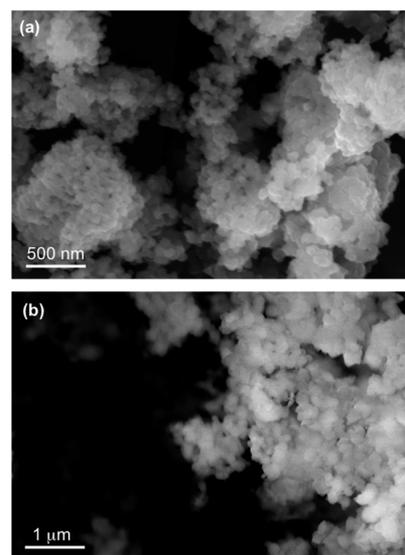

Figure 4. SEM images for (a) polycatechol and (b) polyguaiacol collected on copper grids after a 90 min dark reaction of catechol with FeCl$_3$ at pH 3 in a 1:2 molar ratio.

either catechol or guaiacol solutions (Figure 5). Particles grew to average diameters on the order of a micron, which is consistent
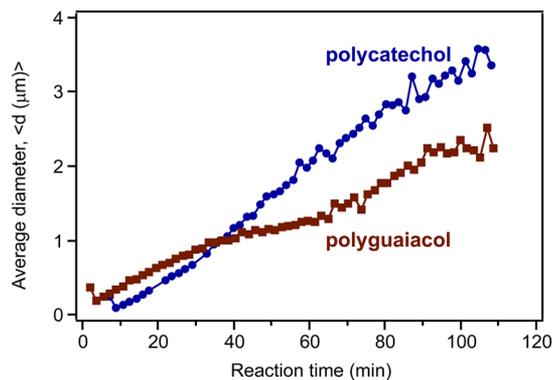

Figure 5. DLS measurements of the average particle size of polycatechol and polyguaiacol as a function of reaction time during the dark reaction of catechol with FeCl$_3$ at pH 3 in a 1:2 molar ratio.

with SEM images, after 30 min of reaction time when sedimentation becomes important. Also at this time, polycatechol particles became larger in average diameter than polyguaiacol particles because of the 1.8× faster growth rate of polycatechol (36 nm/min) compared to that of polyguaiacol particles (20 nm/min). These results suggest that these particles are organic in nature and not a precipitate of iron (oxyhydr)-oxides. Mass yield experiments were also performed where particles were collected and extensively washed with Milli-Q water after 120 min reaction of FeCl$_3$ with either catechol or guaiacol (1:2 organic reactant/Fe molar ratio) at pH 3. Polycatechol mass yield was found to be 47 ± 4%, and that of polyguaiacol was 49 ± 14%. This mass yield is comparable to or larger than the typical mass yields of SOA obtained by photooxidation of common volatile organic compounds, such as terpenes,[39] and it is larger than the yields associated with aqueous SOA (aqSOA) photochemical production.[40] Therefore, the iron-catalyzed reactions of catecholates definitely have the potential to produce SOA with high efficiency.

Moreover, Figure S8a (Supporting Information) shows ATR-FTIR spectra of solid polycatechol and polyguaiacol formed in reactions of Fe(III) with catechol and guaiacol. These spectra are compared with those recorded for aqueous phase catechol[28] and guaiacol (Figure S8b, Supporting Information). There are clear differences between the spectra of monomers and polymers in the 2000−1000 cm^{-1} spectral range containing vibrations of aromatic (1640−1400 cm^{-1}), C−O and C−C stretching (1400−1200 cm^{-1}), and C−H bending (1200−1000 cm^{-1}) modes. This is in line with earlier reports on polycatechol using transmission FTIR using KBr pellets,[41,42] where broadening and shift in peak frequencies was observed due to the rigid structure of polymers. The high intensity of features in the range of 1400−1200 cm^{-1} is characteristic of phenylene (C−C) and oxyphenylene (C−O−C) linkages. These spectra show no absorbance around 1700 cm^{-1} indicative of carbonyl (C=O) groups, which were reported for catechol and guaiacol SOA due to reaction with ozone.[22] This clearly shows that particle formation catalyzed by iron proceeds via a different reaction pathway than SOA formation via metal-free atmospheric photo-oxidation reactions.

Oxidative enzymatic polymerization of guaiacol and catechol is well-studied in biochemical and polymer synthesis fields.[17,24,43] Brick-red colored polyguaiacol prepared from the enzymatic oxidation of monomer guaiacol using peroxidase−H$_2$O$_2$ as catalyst was previously characterized because of its usefulness as a model polymer for lignin biodegradation research.[44] In another study,[36] the solid material was collected from the reaction of guaiacol with Fe(III) chloride and Cr(VI) oxide, which was then solubilized for analysis using UV−vis, HPLC and mass spectrometry. In the case of polycatechol formation, enzymes free of metal centers such as peroxidase[45] and laccase[42] were shown to catalyze polymer synthesis in solutions containing hydrogen peroxide and dissolved oxygen, respectively. Mechanistically, these enzymes catalyze C−C coupling and formation of ether (C−O−C) linkages between catechol monomers (Scheme S2, Supporting Information). Because of their unique thermal, structural properties, and ability to form strong charge transfer complexes with metal oxides, polycatechols are exploited in surface modifications as adhesives and coatings over a wide range of organic and inorganic materials.[24,46] For example, chelating abilities of anachelin (produced by cyanobacteria)[19] and mussel adhesive proteins[20,46−49] containing catechol moieties were exploited in modifying TiO$_2$ surfaces via poly(ethylene glycol) to form stable, protein resistant adlayers (i.e., antifouling polymer) desirable in biomedical devices and marine technology. More related to the work presented herein is the use of the catechol derivative dopamine in anchoring functional molecules to iron oxide shell of magnetic nanoparticles.[18,50] To our knowledge, oxidative polymerization of catechol in the presence of Fe(III) and in the absence of any added oxidants has not received attention.

Recently, Shi et al.[51] investigated the dominant mechanism that leads to iron dissolution in dust. Iron-containing dust samples were collected from two sites that represent sources of Saharan and Asian desert dust. The effect of cycling between wet aerosols (i.e., acidic conditions) and cloud droplets (i.e., more neutral pH and lower ionic strength conditions) on dissolved iron concentration was simulated over about 3 h in the dark. The results showed that insoluble iron dissolves readily under the acidic conditions relevant to wet aerosols, whereas under more neutral pH, the dissolved iron precipitates as poorly crystalline nanoparticles. The relative amount of time mineral dust particles spend as either a wet aerosol or in cloud droplets will affect the

amount of bioavailable iron upon deposition after long-range transport. Also, uptake of acids within clouds can also enhance iron dissolution in the droplets or in the residual aerosol formed after droplet evaporation. Herein, we used hematite to simulate acid-driven dissolution of iron (oxyhydr)oxides and followed the reaction of either catechol or guaiacol with the dissolved iron from these samples. Figure 6 shows digital images of the slurry
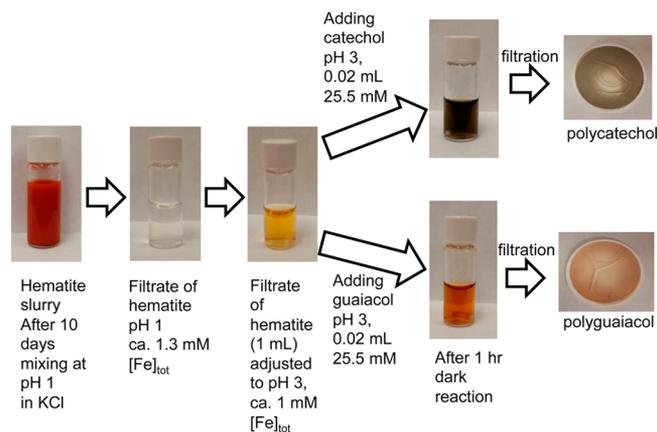

Figure 6. Formation of polycatechol and polyguaiacol from reaction with dissolved iron from acid-promoted hematite dissolution.

and filtrates before and after the addition of the organics, in addition to the filters after 1 h reaction. Clearly, the chemistry described above using FeCl$_3$ as a source of dissolved iron is similar to that from simulated aged iron-containing mineral dust particles. As emphasized in the introduction, pathways for particle formation from phenol derivatives are of increased interest to atmospheric chemists. The implications of these findings are summarized in the following section.

To help fill the gap in our understanding of the surface chemistry driven by iron on atmospherically relevant surfaces, we showed that the dark reaction of catechol and guaiacol with Fe(III) under acidic conditions and in the absence of any added oxidants results in the formation of soluble and reactive secondary organics and insoluble polymeric particles. The strong visible light absorption by the resulting soluble products and insoluble polymeric organic material has implications for the climate. More quantitatively, the significance of these results can be assessed with the help of bulk mass-normalized absorption coefficient (MAC) of the organics, which can be calculated from the base-10 absorbance (A), cuvette width (l), and the initial mass concentration of dissolved catechol (C$_{mass}$) as follows:[25]

$$\text{MAC}(\lambda) = \frac{A(\lambda) \times \ln(10)}{l \times C_{mass}} \tag{1}$$

Figure S9 (Supporting Information) shows a MAC plot for the 3 min dark reaction of 1 mM catechol with 2 mM FeCl$_3$ at pH 3 for an unfiltered solution, that is, with both particles and soluble species contributing to the absorption. Even though we have not accounted for scattering by the particles in the solution, which contributes to the background, it is clear that the MAC values at near-UV and visible ($\lambda > 290$ nm) wavelengths can be as high as 2 × 10^4 cm^2 g^{-1}. These values are comparable to those from biomass burning aerosols (10^3−10^4 cm^2 g^{-1}).[52] Therefore, the efficient dark reaction between phenols and Fe has the potential to produce "brown carbon" aerosol by a secondary mechanism, as opposed to the direct production in biomass burning.

Moreover, the colored polymeric particles are colloidal in solution due to their high hydrophobicity. Depending on the amount of "adsorbed water", these polymers could partition to the surface, thus affecting the aerosols' cloud condensation ability[53,54] and chemical reactivity of surfaces particularly toward reactive gas phase oxidants such as ozone,[55] OH,[56,57] N_2O_5, and NO_3,[58] in addition to light-initiated[4] and redox reactions.[59] The dark formation of these particles driven by Fe(III) under acidic conditions represent a potentially important abiotic pathway for in situ polymer and HULIS formation in atmospheric aerosols in the presence of surface water. This secondary pathway is poorly understood relative to formation pathways of SOA,[2] biopolymeric component of dissolved organic carbon,[60] and HULIS.[61,62] HULIS in particular were shown to generate reactive oxygen species such as hydrogen peroxide and superoxide radicals.[63] The chemistry presented herein provides molecular level details to processes that could take place in acidic multicomponent systems containing organics, iron, and chloride.

■ ASSOCIATED CONTENT

Ⓢ Supporting Information

Figures and tables showing spectra and additional data analysis. The Supporting Information is available free of charge on the ACS Publications website at DOI: 10.1021/acs.est.5b01032.

■ AUTHOR INFORMATION

Corresponding Author
*Phone: (519)884-0710, ext.2873. Fax: (519)746-0677. E-mail: halabadleh@wlu.ca.

Present Address
‖Department of Chemistry and Chemical Biology, McMaster University

Author Contributions
⊥These authors contributed equally to the work.

Notes
The authors declare no competing financial interest.

■ ACKNOWLEDGMENTS

■ REFERENCES

(1) Zhang, R.; Khalizov, A.; Wang, L.; Hu, M.; Xu, W. Nucleation and growth of nanoparticles in the atmosphere. *Chem. Rev.* **2012**, *112*, 1957−2011.

(2) Ziemann, P. J.; Atkinson, R. Kinetics, products, and mechanisms of secondary organic aerosol formation. *Chem. Soc. Rev.* **2012**, *41*, 6582−6605.

(3) Lee, S.-S. Atmospheric science: Aerosols, clouds and climate. *Nature Geosci.* **2011**, *4*, 826−827.

(4) George, C.; D'Anna, B.; Herrmann, H.; Weller, C.; Vaida, V.; Donaldson, D. J.; Bartels-Rausch, T.; Ammann, M. Emerging areas in atmospheric photochemistry. In *Atmospheric and Aerosol Chemistry*; McNeill, V. F., Ariya, P. A., Eds.; Springer: Heidelberg, 2012; Vol. *339*, pp 1−54.

(5) Russell, L. M.; Bahadur, R.; Ziemann, P. J. Identifying organic aerosol sources by comparing functional group composition in chamber and atmospheric particles. *Proc. Natl. Acad. Sci. U.S.A.* **2011**, *108*, 3516−3521.

(6) Prather, K. M.; Hatch, C. D.; Grassian, V. H. Analysis of atmospheric aerosols. *Annu. Rev. Anal. Chem.* **2008**, *1*, 485−514.

(7) Rudich, Y.; Donahue, N. M.; Mentel, T. Aging of organic aerosol: Bridging the gap between laboratory and field studies. *Annu. Rev. Phys. Chem.* **2007**, *58*, 321−352.

(8) Suda, S. R.; Petters, M. D.; Yeh, G. K.; Strollo, C.; Matsunaga, A.; Faulhaber, A.; Ziemann, P. J.; Prenni, A. J.; Carrico, C. M.; Sullivan, R. C.; Kreidenweis, S. M. Influence of functional groups on organic aerosol cloud condensation nucleus activity. *Environ. Sci. Technol.* **2014**, *48*, 10182−10190.

(9) Ault, A. P.; Guasco, T. L.; Ryder, O. S.; Baltrusaitis, J.; Cuadra-Rodriguez, L. A.; Collin, D. B.; Ruppel, M. J.; Bertram, T. H.; Prather, K. A.; Grassian, V. H. Inside versus outside: Ion redistribution in nitric acid reacted sea spray aerosol particles as determined by single particle analysis. *J. Am. Chem. Soc.* **2013**, *135*, 14528−14531.

(10) Guasco, T. L.; Cuadra-Rodriguez, L. A.; Pedler, B. E.; Ault, A. P.; Collins, D. B.; Zhao, D.; Kim, M. J.; Ruppel, M. J.; Wilson, S. C.; Pomeroy, R. S.; Grassian, V. H.; Azam, F.; Bertram, T. H.; Prather, K. A. Transition metal associations with primary biological particles in sea spray aerosol generated in a wave channel. *Environ. Sci. Technol.* **2014**, *48*, 1324−1333.

(11) Cwiertny, D. M.; Young, M. A.; Grassian, V. H. Chemistry and photochemistry of mineral dust aerosol. *Annu. Rev. Phys. Chem.* **2008**, *59*, 27−51.

(12) Al-Abadleh, H. A. Review on the bulk and surface chemistry of iron in atmospherically-relevant systems containing humic like substances. *RSC Adv.* **2015**, *5*, 45785−45811.

(13) Finlayson-Pitts, B. J.; Pitts Jr., J. N. *Chemistry of the Upper and Lower Atmosphere*; Academic Press: New York, 2000.

(14) Nguyen, T. B.; Coggon, M. M.; Flagan, R. C.; Seinfeld, J. H. Reactive uptake and photo-fenton oxidation of glycolaldehyde in aerosol liquid water. *Environ. Sci. Technol.* **2013**, *47*, 4307−4316.

(15) Smith, J. D.; Sio, V.; Yu, L.; Zhang, Q.; Anastasio, C. Secondary organic aerosol production from aqueous reactions of atmospheric phenols with an organic triplet excited state. *Environ. Sci. Technol.* **2014**, *48*, 1049−1057.

(16) Ghorai, S. A.; Laskin, A.; Tivanski, A. V. Spectroscopic evidence of keto-enol tautomerism in deliquesced malonic acid particles. *J. Phys. Chem. A* **2011**, *115*, 4373−4380.

(17) Kobayashi, S.; Makino, A. Enzymatic polymer synthesis: An opportunity for green polymer chemistry. *Chem. Rev.* **2009**, *109*, 5288−5353.

(18) Xu, C.; Xu, K.; Gu, H.; Zheng, R.; Liu, H.; Zhang, X.; Guo, Z.; Xu, B. Dopamine as a robust anchor to immobilize functional molecules on the iron oxide shell of magnetic nanoparticles. *J. Am. Chem. Soc.* **2004**, *126*, 9938−9939.

(19) Zurcher, S.; Wackerlin, D.; Bethuel, Y.; Malisova, B.; Textor, M.; Tosatti, S.; Gademann, K. Biomimetic surface modifications based on the cyanobacterial iron chelator anachelin. *J. Am. Chem. Soc.* **2009**, *128*, 1064−1065.

(20) Statz, A. R.; Meagher, R. J.; Barron, A. E.; Messersmith, P. B. New peptidomimetic polymers for antifouling surfaces. *J. Am. Chem. Soc.* **2005**, *127*, 7972−7973.

(21) *NIST Chemistry WebBook*(http://webbook.nist.gov/chemistry/), Henry's law data for catechol and guaiacol. Accessed January 2013.

(22) Ofner, J.; Kruger, H.-U.; Grothe, H.; Schmitt-Kopplin, P.; Whitmore, K.; Zetzsch, C. Physico-chemical characterization of SOA derived from catechol and guaiacol—A model substance for the aromatic fraction of atmospheric HULIS. *Atmos. Chem. Phys.* **2011**, *11*, 1−15.

(23) Elhabiri, M.; Carrer, C.; Marmolle, F.; Traboulsi, H. Complexation of iron(III) by catecholate-type polyphenols. *Inorg. Chim. Acta* **2007**, *360*, 353−359.

(24) Faure, E.; Falentin-Daudre, C.; Jerome, C.; Lyskawa, J.; Fournier, D.; Woisel, P.; Detrembleur, C. Catechols as versatile platforms in polymer chemistry. *Prog. Polym. Sci.* **2013**, *38*, 236−270.

(25) Laskin, A.; Laskin, J.; Nizkorodov, S. A. Chemistry of atmospheric brown carbon. *Chem. Rev.* **2015**, *115* (10), 4335−4382.

(26) Andreae, M. O.; Gelencser, A. Black carbon or brown carbon? The nature of light-absorbing carbonaceous aerosols. *Atmos. Chem. Phys.* **2006**, *6*, 3131−3148.

(27) Minofar, B.; Jungwirth, P.; Das, M. R.; Kunz, W.; Mahiuddin, S. J. Propensity of formate, acetate, benzoate, and phenolate for the aqueous solution/vapor interface: Surface tension measurements and molecular dynamics simulations. *J. Phys. Chem. C* **2007**, *111*, 8242−8247.

(28) Tofan-Lazar, J.; Situm, A.; Al-Abadleh, H. A. DRIFTS studies on the role of surface water in stabilizing catechol-iron(III) complexes at the gas/solid interface. *J. Phys. Chem. A* **2013**, *117*, 10368−10380.

(29) Feng, W.; Nansheng, D. Photochemistry of hydrolytic iron(III) species and photoinduced degradation of organic compounds. A minireview. *Chemosphere* **2000**, *41*, 1137−1147.

(30) Kipton, H.; Powell, J.; Taylor, M. C. Interactions of iron(II) and iron(III) with gallic acid and its homologues: A potentiormetric and spectrophotometric study. *Aus. J. Chem.* **1982**, *35*, 739−756.

(31) Novic, M.; Grgic, I.; Poje, M.; Hudnik, V. Iron-catalyzed oxidation of S(IV) species by oxygen in aqueous solution: Influence of pH on the redox cycling of iron. *Atmos. Environ.* **1996**, *30*, 4191−4196.

(32) Grgic, I.; Dovzan, A.; Bercic, G.; Hudnik, V. The effect of atmospheric organic compounds on the Fe-catalyzed S(IV) autoxidation in aqueous solution. *J. Atmos. Chem.* **1998**, *29*, 315−337.

(33) Albarran, G.; Boggess, W.; Rassolov, V.; Schuler, R. H. Absorption spectrum, mass spectrometric properties, and electronic structure of 1,2-benzoquinone. *J. Phys. Chem. A* **2010**, *114*, 7470−7478.

(34) Hwang, S.; Lee, C.-H.; Ahn, I.-S. Product identification of guaiacol oxidation catalyzed by manganese peroxidase. *J. Ind. Eng. Chem.* **2008**, *14*, 487−492.

(35) Doerge, D. R.; Divi, R. L.; Churchwell, M. I. Identification of the colored guaiacol oxidation product produced by peroxidases. *Anal. Biochem.* **1997**, *250*, 10−17.

(36) Schmalzl, K. J.; Forsyth, C. M.; Evans, P. D. The reaction of guaiacol with iron III and chromium VI compounds as a model for wood surface modification. *Wood Sci. Technol.* **1995**, *29*, 307−319.

(37) Lee-Ruff, E. The organic chemistry of superoxide. *Chem. Soc. Rev.* **1977**, *6*, 195−214.

(38) Greenlee, W. F.; Chism, J. P.; Rickert, D. E. A novel method for the separation and quantitation of benzene metabolites using high-pressure liquid chromatography. *Anal. Biochem.* **1981**, *112*, 367−370.

(39) Lee, A.; Goldstein, A. H.; Keywood, M. D.; Gao, S.; Varutbangkul, V.; Bahreini, R.; Ng, N. L.; Flagan, R. C.; Seinfeld, J. H. Gas-phase products and secondary aerosol yields from the ozonolysis of ten different terpenes. *J. Geophys. Res.* **2006**, *111*, D07302.

(40) Ervens, B.; Turpin, B. J.; Weber, R. J. Secondary organic aerosol formation in cloud droplets and aqueous particles (aqSOA): A review of laboratory, field, and model studies. *Atmos. Chem. Phys.* **2011**, *11*, 11069−11102.

(41) Sun, X.; Bai, R.; Zhang, Y.; Wang, Q.; Fan, X.; Yuan, J.; Cui, L.; Wang, P. Laccase-catalyzed oxidative polymerization of phenolic compounds. *Appl. Biochem. Biotechnol.* **2013**, *171*, 1673−1680.

(42) Aktas, N.; Shahiner, N.; Kantoglu, O.; Salih, B.; Tanyolac, A. Biosynthesis and characterization of laccase catalyzed poly(catechol). *J. Polym. Environ.* **2003**, *11*, 123−128.

(43) Monti, D.; Ottolina, G.; Carrea, G.; Riva, S. Redox reactions catalyzed by isolated enzymes. *Chem. Rev.* **2011**, *111*, 4111−4140.

(44) Crawford, R. L.; Robinson, L. E.; Foster, R. D. Polyguaiacol: A useful model polymer for lignin biodegradation research. *Appl. Environ. Microbiol.* **1981**, *41*, 1112−1116.

(45) Dubey, S.; Singh, D.; Misra, R. A. Enzymatic synthesis and various properties of poly(catechol). *Enzyme Microb. Technol.* **1998**, *23*, 432−437.

(46) Ye, Q.; Zhou, F.; Liu, W. Bioinspired catecholic chemistry for surface modification. *Chem. Soc. Rev.* **2011**, *40*, 4244−4258.

(47) Lee, H.; Dellatore, S. M.; Miller, W. M.; Messersmith, P. B. Mussel-inspired surface chemistry for multifunctional coatings. *Science* **2007**, *318*, 426−430.

(48) Dalsin, J. L.; Hu, B.-H.; Lee, B. P.; Messersmith, P. B. Mussel adhesive protein mimetic polymers for the preparation of nonfouling surfaces. *J. Am. Chem. Soc.* **2003**, *125*, 4253−4258.

(49) Dalsin, J. L.; Lin, L.; Tosatti, S.; Voros, J.; Textor, M.; Messersmith, P. B. Protein resistance of titanium oxide surfaces modified by biologically inspired MPEG−DOPA. *Langmuir* **2005**, *21*, 640−646.

(50) Zhou, W.-H.; Lu, C.-H.; Guo, X.-C.; Chen, F.-R.; Yang, H.-H.; Wang, X.-R. Mussel-inspired molecularly imprinted polymer coating superparamagnetic nanoparticles for protein recognition. *J. Mater. Chem.* **2010**, *20*, 880−883.

(51) Shi, Z.; Krom, M. D.; Bonneville, S.; Benning, L. G. Atmospheric processing outside clouds increases soluble iron in mineral dust. *Environ. Sci. Technol.* **2015**, *49*, 1472−1477.

(52) Chen, Y.; Bond, T. C. Light absorption by organic carbon from wood combustion. *Atmos. Chem. Phys.* **2010**, *10*, 1773−1787.

(53) Taraniuk, I.; Graber, E. R.; Kostinski, A.; Rudich, Y. Surfactant properties of atmospheric and model humic-like substances (HULIS). *Geophys. Res. Lett.* **2007**, *34*, L16807 DOI: 10.1029/2007GL029576.

(54) Dinar, E.; Taraniuk, I.; Graber, E. R.; Anttila, T.; Mentel, T. F.; Rudich, Y. Hygroscopic growth of atmospheric and model humic-like substances. *J. Geophys. Res.: Atmos.* **2007**, *112*, D05211 DOI: 10.1029/2006JD007442.

(55) Nieto-Gligorovski, L. I.; Net, S.; Gligorovski, S.; Wortham, H.; Grothe, H.; Zetzsch, C. Spectroscopic study of organic coatings on fine particles, exposed to ozone and simulated sunlight. *Atmos. Environ.* **2010**, *44*, 5451−5459.

(56) Bertram, A. K.; Ivanov, A. V.; Hunter, M.; Molina, L. T.; Molina, M. J. The reaction probability of OH on organic surfaces of tropospheric interest. *J. Phys. Chem. A* **2001**, *105*, 9415−9421.

(57) George, I. J.; Slowik, J.; Abbatt, J. P. D. Chemical aging of ambient organic aerosol from heterogeneous reaction with hydroxyl radicals. *Geophys. Res. Lett.* **2008**, *35*, L13811 DOI: 10.1029/2008GL033884.

(58) Gross, S.; Bertram, A. K. Reactive uptake of NO_3, N_2O_5, NO_2, HNO_3, and O_3 on three types of polycyclic aromatic hydrocarbon surfaces. *J. Phys. Chem. A* **2008**, *112*, 3104−3113.

(59) Duesterberg, C. K.; Waite, T. D. Kinetic modeling of the oxidation of *p*-hydroxybenzoic acid by Fenton's reagent: Implications of the role of quinones in the redox cycling of iron. *Environ. Sci. Technol.* **2007**, *41*, 4103−4110.

(60) Aluwihare, L. I.; Repeta, D. J.; Chen, R. F. A major biopolymeric component to dissolved organic carbon in surface sea water. *Nature* **1997**, *387*, 166−169.

(61) Graber, E. R.; Rudich, Y. Atmospheric HULIS: How humic-like are they? A comprehensive and critical review. *Atmos. Chem. Phys.* **2006**, *6*, 729−753.

(62) Noziere, B.; Dziedzic, P.; Cordova, A. Formation of secondary light-absorbing "fulvic-like" oligomers: A common process in aqueous and ionic atmospheric particles? *Geophys. Res. Lett.* **2007**, *34*, L21812 DOI: 10.1029/2007GL031300.

(63) Lin, P.; Yu, J. Z. Generation of reactive oxygen species mediated by humic-like substances in atmospheric aerosols. *Environ. Sci. Technol.* **2011**, *45*, 10362−10368.